

The implications of the H₂ variability in Titan's exosphere

J. Cui,^{1,2} R. V. Yelle,³ I. C. F. Müller-Wodarg,⁴ P. P. Lavvas,³ and M. Galand⁴

Received 5 May 2011; revised 6 August 2011; accepted 12 September 2011; published 19 November 2011.

[1] We present in this paper an investigation of the distribution of H₂ in Titan's exosphere, based on the measurements made with the Ion Neutral Mass Spectrometer (INMS) onboard Cassini during 32 encounters with the satellite. The observed H₂ density in Titan's exosphere shows significant variance from flyby to flyby. However, no appreciable trend with geophysical or solar conditions can be identified. A data-model comparison is made in the framework of the Chamberlain approach, taking into account two ideal cases. First, we assume that the observed variability is spatial. In this case, the damping of exobase perturbations when propagating into the exosphere is a diagnostic of the spatial scale of the perturbations. We find that for all reasonable choices of this spatial scale, the model predicts significantly more damping than implied by the INMS data. Second, we assume that at any given time, the physical conditions in Titan's upper atmosphere and exosphere are globally uniform, but these conditions evolve with time, indicating that the observed variability is temporal. In such a case, the observations can be interpreted as a result of exobase perturbations on timescales in the range of $\sim 10^3$ – 10^6 s. The time-varying H₂ exosphere of Titan essentially reflects the varying structure and energy deposition in the upper atmosphere of the satellite, which are ultimately determined by the variations in either the solar EUV/UV radiation or the level of magnetospheric particle precipitation. However, we do not expect the considerable variability observed for Titan's H₂ exosphere to be induced by the varying solar inputs into Titan's atmosphere. Instead, we postulate that such a variability is more likely to be associated with Titan's varying plasma environment. Comparisons between different categories of Titan flybys tentatively reveal that the H₂ exosphere tends to be more energetic and more expanded, and H₂ molecules tend to escape more rapidly, with increasing levels of electron precipitation from the ambient plasma environment.

Citation: Cui, J., R. V. Yelle, I. C. F. Müller-Wodarg, P. P. Lavvas, and M. Galand (2011), The implications of the H₂ variability in Titan's exosphere, *J. Geophys. Res.*, 116, A11324, doi:10.1029/2011JA016808.

1. Introduction

[2] An exosphere is commonly referred as the uppermost part of the planetary atmosphere, where the collision frequency becomes so low that particles essentially undergo free-streaming motion under the gravitational influence of the central body. In the traditional framework that assumes a sharp transition between collisional and collisionless states, the gas distribution in the exosphere is completely determined by the physical conditions at the lower boundary, i.e., the exobase [Johnson *et al.*, 2008, and references therein]. In the seminal work of Chamberlain [1963], a uniform exobase was

assumed, with the particle velocity distribution function (hereafter VDF) taken to be Maxwellian. The exospheric density was then determined with a kinetic approach by integrating the Maxwellian VDF over truncated regions of the momentum space.

[3] The above simple case was later extended to allow for horizontal variations in the exobase density and temperature [e.g., Vidal-Madjar and Bertaux, 1972; Hartle, 1973], typically parameterized with empirical models such as that of Jacchia [1971]. The propagation of exobase variations into the exosphere is naturally implied by such a kinetic model. The magnitude of the variations, however, is significantly damped in the exosphere, since the ballistic flux and the associated lateral heat transfer help to remove any existing variance in density and temperature, driving the conditions near or above the exobase toward uniformity [e.g., Fahr, 1970]. The propagation of exobase variations into the exosphere has been studied extensively for the Earth and supported by satellite observations of geocoronal emission [e.g., Meier and Mange, 1970]. It has also been evaluated for other Solar System bodies such as Mars [Kim and Son, 2000].

[4] Following the above line of reasoning, we investigate in this paper the density variations in Titan's exosphere, by

¹Department of Astronomy and Key Laboratory of Modern Astronomy and Astrophysics, Ministry of Education, Nanjing University, Nanjing, China.

²National Astronomical Observatories, Chinese Academy of Sciences, Beijing, China.

³Lunar and Planetary Laboratory, University of Arizona, Tucson, Arizona, USA.

⁴Space and Atmospheric Physics Group, Department of Physics, Imperial College London, London, UK.

virtue of the extensive measurements made during the Cassini flybys with the satellite. Titan's exosphere is primarily composed of molecular hydrogen (H₂), methane (CH₄) and molecular nitrogen (N₂). We focus on H₂ in this work, the distribution of which can be reasonably reproduced by the traditional Chamberlain model [Cui *et al.*, 2008]. The cases for CH₄ and N₂, however, are more complicated, as the investigations of De La Haye *et al.* [2007a, 2007b] have revealed the presence of suprathermal CH₄ and N₂ coronae on Titan, with the Maxwellian VDF providing poor fits to the data.

[5] The structure of the paper is as follows. In section 2, we present the observed variations of H₂ density above Titan's exobase, based on the in-situ measurements made by Cassini during its Titan flybys. We show in section 3 that the observations cannot be reproduced by the simple kinetic model assuming that the observed variations are spatial. We investigate the validity of such a model in section 4, where we propose that the observed H₂ variation in Titan's exosphere is more likely a temporal phenomenon. This is followed by a discussion of the possible implications of the INMS H₂ observations in section 5. Finally, we conclude in section 6.

2. Observations of a Variable H₂ Exosphere From Cassini INMS Measurements

[6] The H₂ densities in Titan's exosphere were measured in-situ by the Cassini Ion Neutral Mass Spectrometer (INMS) when operating in the Closed Source Neutral (CSN) mode [Waite *et al.*, 2004]. Until now, there have been over 70 Titan flybys for which the INMS neutral data are available. The H₂ densities are obtained from count rates recorded in mass channel 2, with thruster firing contamination removed and background signals subtracted. Only measurements with INMS-favored spacecraft configurations (here defined with ram angles less than 60°) are considered in this study. The procedures of data analysis have been detailed by Yelle *et al.* [2006], Cui *et al.* [2008, 2009] and Magee *et al.* [2009] and thus are not repeated here. We have also taken into account an average enhancement factor of ~2.6, required to match the INMS total densities to the Huygens Atmosphere Structure Instrument (HASI) values as well as those inferred from the Cassini Attitude and Articulation Control Subsystem (AACS) [Strobel, 2010]. Throughout this study, we will not use the H₂ measurements made at altitudes above ~4000 km, where a significant fraction of the channel 2 count is contaminated by the residual H₂ gas in the INMS chamber. Below this altitude, the density of the residual gas is typically lower than the uncertainty of the atmospheric density.

[7] To be conservative, outbound measurements are excluded in our analysis due to possible wall effect, which is clearly seen from the asymmetry between the average inbound and outbound H₂ density profiles above Titan's exobase [Cui *et al.*, 2008]. Such an instrumental effect refers to the processes of adsorption/desorption or surface chemical reactions that take place on the INMS chamber walls [Vuitton *et al.*, 2008; Cui *et al.*, 2009]. However, it is worth emphasizing that the above argument relies on the assumption of identical sampling of Titan's upper atmosphere and exosphere for both the inbound and outbound flybys, which is not exactly true. Despite this, we note that the main results of this

paper are still valid even with the inbound INMS H₂ data included in the analysis.

[8] The INMS sample appropriate for this study combines the data acquired during 32 flybys of Cassini with Titan (from T5 to T71). The sample is significantly larger than that adopted for our previous investigation of the global average H₂ distribution [Cui *et al.* [2008], including 14 flybys from T5 to T32). Among these 32 flybys, 24 of them provide continuous INMS neutral measurements for Titan's thermospheric and exospheric regions from the closest approach up to at least ~4000 km above the surface. The data from the remaining 8 flybys in our sample contain gaps near or below the exobase, but still provide useful measurements of the H₂ content in Titan's lower exosphere. Other flybys, though with neutral data available, have been excluded here either due to spacecraft configurations not favored for INMS neutral observations (i.e., with ram angles greater than 60°), or due to closest approach altitudes being too high (i.e., above 4,000 km).

[9] To simplify the discussions below, we place Titan's exobase at a common altitude of 1500 km above the surface in this and the following sections, to be consistent with the choice of Cui *et al.* [2008]. In section 5, we allow a variable exobase height from flyby to flyby, and calculations there validate our assumption of a common exobase height at 1500 km. It is also worth mentioning that strictly speaking, the exobase should be understood as an extended transition region rather than a rigid surface, since H₂ escapes from Titan not exactly with the limiting flux [Strobel, 2009]. However, the main conclusions of this paper are not sensitive to the assumption of a sharp transition at the exobase.

2.1. Lack of Appreciable Horizontal Trend

[10] At any given altitude in Titan's exosphere, we have tried to search for the variations in H₂ density with latitude, longitude, local solar time, and/or solar zenith angle. Variations with latitude have been identified in Titan's thermosphere, for both CH₄ and H₂, characterized by clear depletion near the equator [Müller-Wodarg *et al.*, 2008; Cui *et al.*, 2009]. Variations with longitude, local solar time and solar zenith angle have not been confirmed in previous investigations when taking into account possible contamination by biased sampling and instrumental effects [Cui *et al.*, 2009]. Despite this, the diurnal variation has been predicted by Thermospheric Global Circulation Model (TGCM) calculations [Müller-Wodarg *et al.*, 2000; Müller-Wodarg and Yelle, 2002], while the longitudinal variation could be associated with significant energy deposition through electron/ion precipitation from Saturn's magnetosphere [e.g., Sittler *et al.*, 2010; Bell *et al.*, 2011]. Indeed, it has been proposed that Saturn's magnetospheric inputs may provide an appreciable contribution to the ionization of neutral particles in Titan's upper atmosphere, especially at the nightside [e.g., Ågren *et al.*, 2007; Cravens *et al.*, 2008a, 2008b], and the thermospheric response of Titan to its plasma environment has recently been investigated by Westlake *et al.* [2011].

[11] As an example, we show in Figure 1 (top and middle) the H₂ density as a function of latitude, at 1500 km (the exobase) and 2500 km, respectively. The figure shows that no convincing meridional variation can be observed. Investigations of the zonal and diurnal variations in exospheric H₂

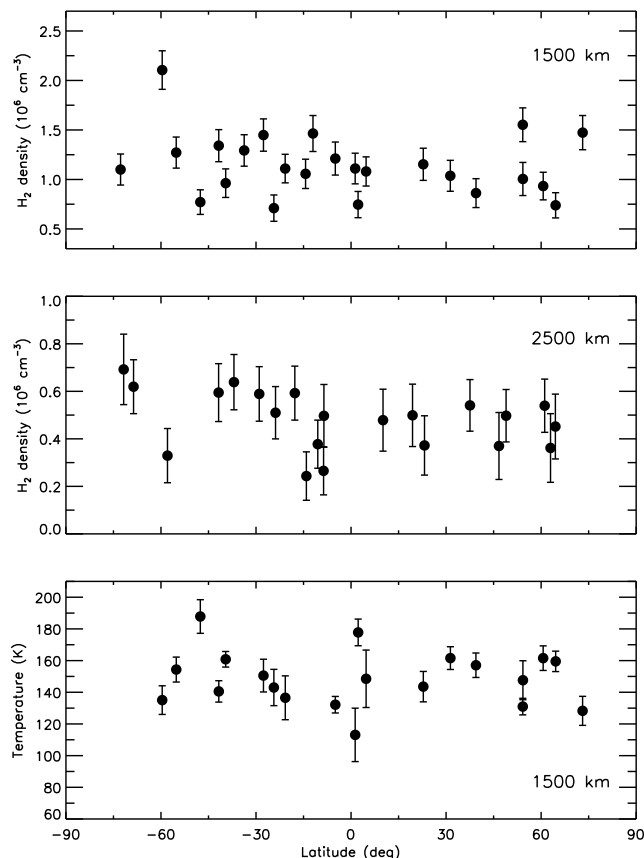


Figure 1. The meridional variation of H₂ density at (top) 1500 km (the exobase) and (middle) 2500 km, combining the INMS measurements made during all available Titan flybys. (bottom) Also shown is the meridional variation of exobase temperature. Vertical bars in all panels are associated with counting statistics. No appreciable horizontal trend is identified in either H₂ density or exobase temperature.

density give similar results. At the face value, the absence of any horizontal trend in Titan's exosphere may not be surprising, since any exospheric region is occupied by particles from different parts of the exobase following their trajectories. As a consequence, density in the exosphere tends to reflect the global average physical conditions at the exobase, and any possible variation in thermospheric density and temperature tends to be smoothed out when propagating upward.

[12] In Figure 1 (bottom), we show the meridional variation of exobase temperature derived from the INMS N₂ data. The information on exobase temperature is required to calculate Titan's exospheric H₂ distribution within the framework of the traditional Chamberlain model (see section 3). The derivation of exobase temperature requires some reasonable assumption about the neutral distribution in Titan's atmosphere [e.g., Westlake *et al.*, 2011]. Here we assume isothermal conditions throughout Titan's upper thermosphere and derive a unique temperature based on the INMS measurements of N₂ made during any single flyby, but treating inbound and outbound data separately [e.g., De La Haye *et al.*, 2007a; Cui *et al.*, 2008, 2009; Westlake *et al.*, 2011].

From the figure, we see that no significant meridional trend can be identified, similar to the observations of H₂ density.

[13] Despite the lack of any appreciable trend with geophysical or solar conditions as shown in Figure 1, we note that both the H₂ density and the thermospheric temperature present considerable variance from flyby to flyby. Such a variance is significantly larger than that allowed by counting statistics, especially at low altitudes. For further investigation, it is interesting to compare the density profiles obtained during different flybys with similar spacecraft trajectory geometry. An example is given in Figure 2, which shows the exospheric H₂ distribution obtained during the inbound passes of T18 (the black solid line) and T19 (the gray dotted line). At the altitudes shown in the figure, both flybys probe high latitude regions of the northern hemisphere, magnetospheric wakeside, as well as Titan local time near the morning terminator. However, there is clearly a difference between the H₂ density profiles for these two flybys in that the densities obtained during inbound T18 are systematically higher than those obtained during inbound T19. Similar conclusions for other flyby groupings have been reported by Westlake *et al.* [2011], with differences in thermospheric temperature being as large as ~30 K for roughly identical solar and geophysical conditions.

2.2. Parameterization of Variability

[14] We have shown above that the observed H₂ density and exobase temperature do not show clear evidence of horizontal trend, but significant variability is present from flyby to flyby. In this section, we investigate further how such a variability evolves with altitude in Titan's exosphere. We will show below that such information could be used to probe the nature of the density and temperature perturbations in Titan's thermosphere.

[15] The simplest way to parameterize the H₂ density variability is to calculate the standard deviation of all measurements

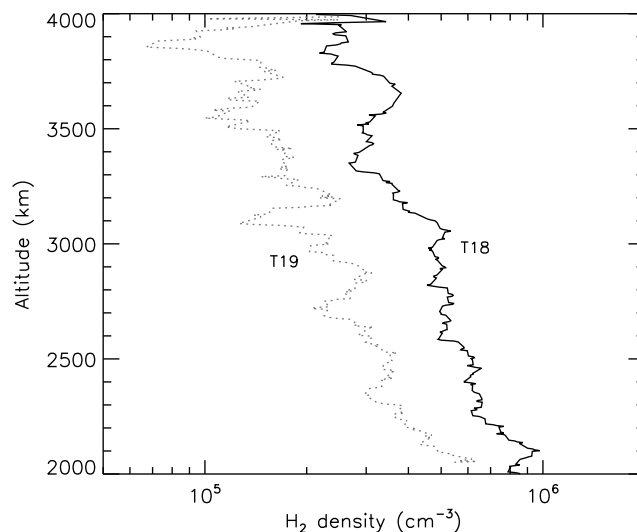


Figure 2. The H₂ density profiles in Titan's exosphere obtained during the inbound T18 and T19 flybys. These two flybys have similar trajectory geometry but present significant density variance.

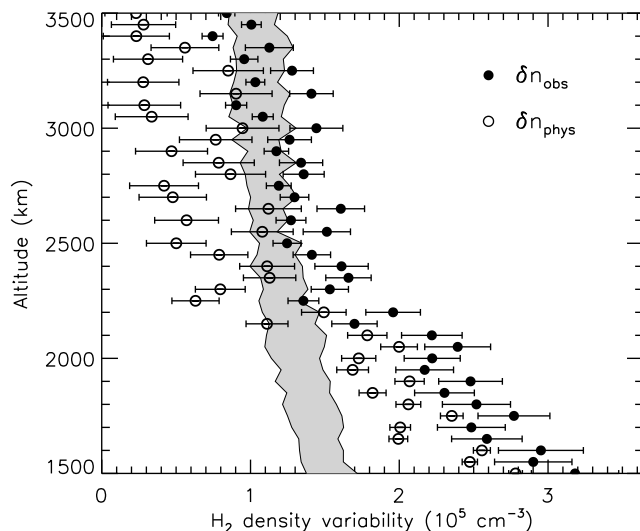


Figure 3. The altitude dependence of the observed variability, δn_{obs} (the solid circles), and the variability due to counting statistics (the shadowed region) in exospheric H₂ density. The observed variability is appreciably larger than that allowed by counting statistics below ~ 2500 km. The open circles give the physical variability, δn_{phys} , as a function of altitude, constructed by assuming lognormal distribution and deconvolving the observed variability with a Gaussian kernel function representing statistical degradation (see section 2.2 for details).

made at any given altitude. However, there is a complexity in such a procedure since the standard deviation directly obtained from the data reflects the convolution of the physical variability with a kernel function (to be detailed later) representing data degradation due to counting statistics. To illustrate this, we show with the solid circles in Figure 3 the altitude dependence of the observed variability in H₂ density, δn_{obs} , above Titan's exobase, defined as the standard deviation of H₂ density measurements at any given altitude extracted from all available flybys in our sample. For comparison, the observed variability is overlotted on the variability associated with statistical degradation. This corresponds to the shadowed region encompassed by two solid lines calculated from the mean of all density errors at any given altitude plus/minus the standard deviation of the density error. From Figure 3, counting statistics makes a significant contribution to, but cannot fully account for, the observed variability. Therefore as the first step, it is necessary to remove the variance associated with statistical degradation.

[16] To recover the physical variability, δn_{phys} , from the raw data, we make some reasonable assumption on the functional form of the probability distribution of H₂ density at any given altitude. We show in Figure 4 the H₂ probability distribution at the exobase. We see that the density distribution is not symmetric about the maximum, characterized by a high density tail above $\sim 1.5 \times 10^6 \text{ cm}^{-3}$. Similar features are observed at higher altitudes, indicating that symmetric functional forms such as Gaussian are not appropriate. Instead, we find that the convolution of a lognormal probability distribution with the kernel function (associated with statistical degradation) is a reasonable representation of the INMS observations. Here the kernel function is assumed to be

Gaussian with the width taken from the mean 1σ uncertainty of individual measurements. The lognormal distribution, used to characterize the physical probability distribution of H₂ density, can be expressed as

$$P(n) = \frac{1}{n\sigma\sqrt{2\pi}} e^{-\frac{\ln n - \mu}{2\sigma^2}}, \quad (1)$$

where n is the H₂ density, μ and σ are two parameters that determine all statistical quantities such as the mean value ($e^{\mu + \sigma^2/2}$) and standard deviation ($\sqrt{e^{\sigma^2} - 1} e^{\mu + \sigma^2/2}$). In Figure 4, the best-fit exobase H₂ distribution is given by the dashed line, corresponding to the convolution of the true (lognormal) distribution (given by the solid line) with the Gaussian kernel representing counting statistics. Both curves have been scaled to match the total number of density measurements at that particular altitude.

[17] The physical variability in exospheric H₂ density, δn_{phys} , defined here as the standard deviation of the lognormal distribution, is shown by the open circles in Figure 3 as a function of altitude. This variability is dominant over the variability due to counting statistics at relatively low altitudes, suggesting propagation of exobase perturbations well into Titan's exosphere. However, the physical variability decreases appreciably with increasing altitude, and eventually falls below the noise level above ~ 2000 km.

[18] The physical variability in H₂ density derived from the data will be compared with simple kinetic model calculations in section 3. Such calculations also rely on the choice of the neutral temperature variability at the exobase. This is modeled with a Gaussian distribution with a mean of 141 K and a standard deviation of 20 K. The above mean exobase temperature is lower than the value of ~ 150 K reported by previous INMS works [e.g., Yelle *et al.*, 2006; Cui *et al.*, 2008; Müller-Wodarg *et al.*, 2008], but consistent with the more

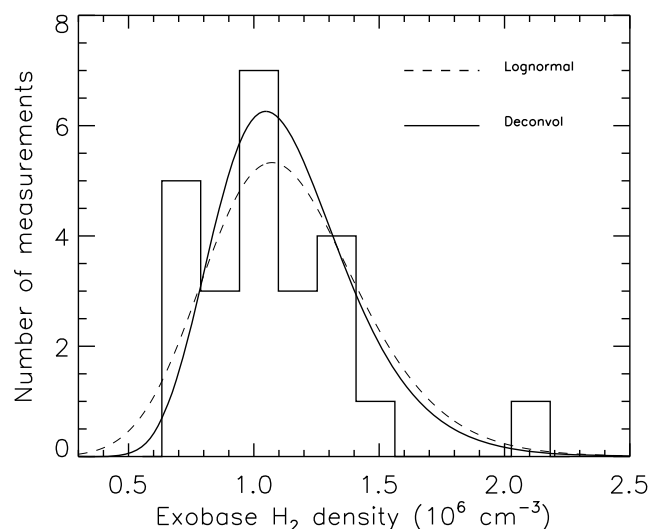


Figure 4. The probability distribution of H₂ density at Titan's exobase. The solid histogram shows the observed distribution, and the solid curve gives the physical distribution, recovered by assuming lognormal. For comparison, we show with the dashed line the convolution of the physical (lognormal) distribution with a Gaussian kernel characterizing data degradation due to counting statistics.

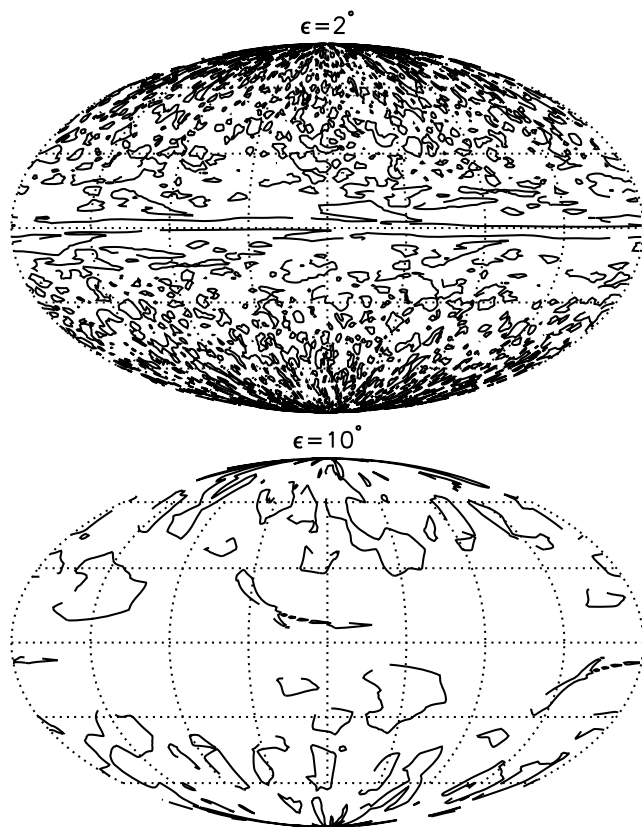


Figure 5. Random realizations of the exobase density for an angular resolution of (top) 2° and (bottom) 10° . These correspond to a horizontal spatial scale of ~ 140 km and ~ 700 km at the exobase. For simplicity, only the contour with H₂ density 20% higher than the mean exobase value is drawn.

recent value of 140.4 K from *Westlake et al.* [2011]. This is primarily a result of significantly more INMS data included in the present work (and that of *Westlake et al.* [2011]). At the exobase, the relative uncertainty (due to counting statistics) in neutral temperature ($\sim 5\%$) is significantly smaller than that in H₂ density ($\sim 15\%$). As a consequence, data degradation by counting statistics causes only a slight increase (by less than 1 K) in the observed variability of exobase temperature, as compared with the true physical variability. Such a minor effect is ignored in this study.

[19] Finally, we emphasize that here the variations of exobase density and temperature are sampled independently, despite a possible anti-correlation between the two quantities (see section 5 for details). However, we have run test models to ensure that such an effect does not influence the main results of this paper significantly.

3. Propagation of Spatial Exobase Perturbations Into the Exosphere From the Chamberlain Approach

[20] In this section, we evaluate the density variability in Titan's H₂ exosphere in the framework of the collisionless Chamberlain approach. We assume that the physical conditions near or above the exobase are static, which means that the observed variability is a spatial feature without any tem-

poral effect (however, see section 4.2 for an alternative approach).

[21] Calculations of exospheric H₂ densities on Titan rely on the choice of the density and temperature distributions at the exobase. Due to the lack of any appreciable horizontal trend as discussed in section 2.1, the exobase density and temperature distributions are modeled with random realizations of the physical variability of these quantities (normal for temperature and lognormal for density, see section 2.2). The random samplings of exobase density and temperature rely on the detailed choice of the horizontal spatial scale of the perturbations. On the one hand, consecutive measurements made during any single flyby always present smooth profiles. This indicates that the scale of the perturbations should be significantly larger than the distance traveled by the spacecraft over the time interval of one full INMS mass scan, i.e., ~ 5.5 km [*Cui et al.*, 2009]. On the other hand, the horizontal scale crossed by two different flybys with similar spacecraft trajectories but significant density variance (such as the inbound T18 and T19, see section 2.1) is typically ~ 800 km at the exobase. Therefore in principle, the scale of the exobase density and temperature perturbations allowed by the data could have a large range from ~ 10 km to $\sim 10^3$ km, depending on the mechanism that drives these perturbations.

[22] In the following, we describe how the exobase structures are sampled. The general idea is to divide Titan's exobase into cells, with density and temperature distributions defined by physical values derived from the INMS data and placed in random spatial locations. The exobase perturbations are then used to evaluate their propagation into the exosphere within the framework of the Chamberlain approach. More specifically, we denote the angular resolution of the exobase perturbations with ϵ (as viewed from Titan's center) throughout this paper. For a given value of ϵ , we throw a total number of $N \approx 4\pi/[\pi(\epsilon/2)^2]$ uniformly distributed random positions across Titan's exobase, where ϵ is in units of radian. This is accomplished by sampling azimuthal angles, α , with $\alpha = \pi(2R_1 - 1)$ and meridional angles, δ , with $\delta = \cos^{-1}(2R_2 - 1)$, where R_1 and R_2 are two independent random numbers uniformly distributed between 0 and 1. We attribute values of H₂ density and neutral temperature to these random points, and values at intermediate positions are obtained by natural neighbor interpolation. We require that the resulting density distribution be consistent with the true physical distribution of exobase density as constructed from lognormal-based deconvolution. Random sampling of the temperature field on Titan's exobase is accomplished in a similar manner, but based on the assumption of normal distribution.

[23] Since the random realization of exobase conditions is an important part of our model calculations, several points need to be clarified. (1) The angular resolution of the exobase perturbations, ϵ , is treated as a free parameter in this study, and the choice of this value is an essential element of the random sampling since it determines how fast the density variability is damped when propagating into the exosphere (see below for details). (2) The physical values (density and temperature) attributed to the randomly selected N positions are constrained by the observations and are independent of ϵ . (3) Density and temperature values at intermediate positions are required for performing numerical integration, especially when ϵ is large. These values are obtained from numerical

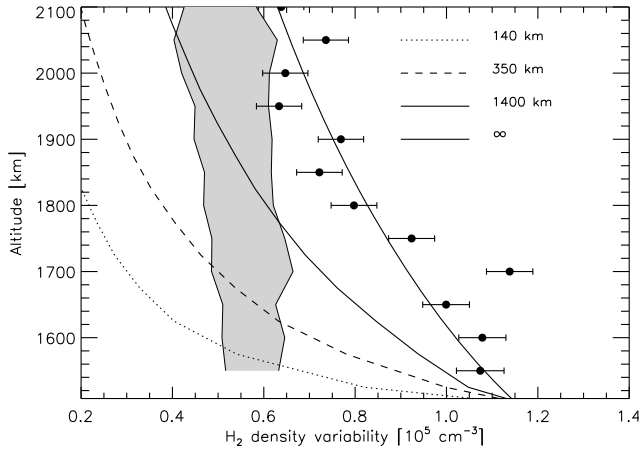


Figure 6. The altitude dependence of H₂ density variability in Titan's exosphere, overplotted on the INMS observations (with contribution from statistical degradation removed). For comparison, the variability due to statistical degradation is also given with the drawing conventions of Figure 3. Several different model cases are shown, corresponding to different horizontal scales of the density and temperature perturbations on Titan's exobase.

interpolation instead of direct random sampling, since the latter effectively reduces the scale of the perturbations.

[24] Two examples of the random realization of the exobase density are shown in Figure 5 as the ellipsoidal projection of two-dimensional contours. The H₂ density field given in Figure 5 (top) has an angular resolution of $\epsilon \sim 2^\circ$ (corresponding to a horizontal spatial scale of ~ 140 km at the exobase) and that in Figure 5 (bottom) has $\epsilon \sim 10^\circ$ (corresponding to a horizontal spatial scale of ~ 700 km at the exobase). To improve visibility, only the contour with H₂ density 20% higher than the mean exobase value is drawn. It is evident from the figure that a smaller angular resolution for the random sampling is reflected by more complicated density structures.

[25] To calculate the exospheric density structure from the exobase conditions, it is convenient to define two dimensionless quantities, $y = r_{\text{exo}}/r$ and $V = v/v_{\text{esc}}$, where r is the radial distance, v is the particle velocity, r_{exo} is the exobase radius, and v_{esc} is the escape velocity at Titan's exobase. We calculate the exospheric H₂ densities as a function of altitude (or equivalently, dimensionless parameter y), meridional angle (δ) and azimuthal angle (α), by evaluating the following integrals numerically using 20 points Gaussian quadrature,

$$\begin{aligned}
 N_b(y, \alpha, \delta) = & m^3 v_{\text{esc}}^3 \int_0^{V_b} V^2 dV \int_0^\pi \sin \theta d\theta \int_0^{2\pi} f_{\text{exo}} d\phi \\
 & + m^3 v_{\text{esc}}^3 \int_{V_b}^{\sqrt{y}} V^2 dV \int_0^{\theta_m} \sin \theta d\theta \int_0^{2\pi} f_{\text{exo}} d\phi \\
 & + m^3 v_{\text{esc}}^3 \int_{V_b}^{\sqrt{y}} V^2 dV \int_{\pi-\theta_m}^\pi \sin \theta d\theta \int_0^{2\pi} f_{\text{exo}} d\phi, \quad (2)
 \end{aligned}$$

$$N_h(y, \alpha, \delta) = m^3 v_{\text{esc}}^3 \int_{\sqrt{y}}^\infty V^2 dV \int_0^{\theta_m} \sin \theta d\theta \int_0^{2\pi} f_{\text{exo}} d\phi, \quad (3)$$

where $f_{\text{exo}}(V, \theta, \phi)$ is the H₂ VDF at Titan's exobase assumed to be Maxwellian, m is the mass of H₂ molecules, θ and ϕ are meridional and azimuthal angles in the velocity space [Vidal-Madjar and Bertaux, 1972]. Equations (2) and (3) give the exospheric densities of ballistic and hyperbolic particles, respectively. Satellite particles are ignored in this study, since in any collisionless model there is no mechanism to establish a steady population of these particles [Cui et al., 2008]. According to Vidal-Madjar and Bertaux [1972], the integral limits in equations (2) and (3) can be written as $V_b = y/\sqrt{1+y}$ and $\sin \theta_m = (y\sqrt{V^2+1-y})/V$. Finally, for any given particle trajectory (represented by the six trajectory parameters: $y, \delta, \alpha, V, \theta, \phi$), f_{exo} should be evaluated with the meridional and azimuthal angles corresponding to where the trajectory intersects the exobase. The dependence of their values on trajectory parameters can be established based on geometrical and dynamical considerations [Vidal-Madjar and Bertaux, 1972, equations 13 and 14] and are not detailed here.

[26] The model calculations of the H₂ density variability in Titan's exosphere, calculated from equations (2) and (3) above, are shown in Figure 6 as a function of altitude and overplotted on the INMS observations (the solid circles with error bars). The contribution from statistical degradation has been removed from the data. Different line styles represent calculations made with different assumptions about the scale of the exobase perturbations, from as small as 140 km to as large as 1400 km (corresponding to different ϵ values). A total number of 10,000 random samplings are calculated for each case. For comparison, we also show in Figure 6 the variability due to counting statistics alone, with the drawing conventions of Figure 3. To better simulate the sampling of the INMS data, the model variability is determined by extracting model densities at exactly the same altitude, meridional angle and azimuthal angle as those from the data. The random nature of the sampling implies that using longitude or local solar time to represent the azimuthal angle makes negligible difference to the simulated results.

[27] Figure 6 shows that there is a remarkable difference between the 140 km model and the data. The INMS observations suggest that the perturbations at the exobase propagate well into Titan's exosphere. In contrast, the model results show sharp decrease of the density variability within a narrow region of width ~ 50 km above the exobase. Except very close to the exobase, the model variability in H₂ density falls below the statistical noise. With a larger scale of 350 km for the exobase perturbations, the density variability decreases more slowly with increasing altitude, as shown in Figure 6. This is because the H₂ density and temperature over the same region of Titan's exobase tend to be more structured when the scale of perturbations is smaller, thus the exobase perturbations are more easily damped when propagating into the exosphere. As the scale of the exobase perturbations increases further to ~ 1400 km, the agreement between the data and the model becomes better. Despite this, the model profile still appears to be under-estimated as compared to the INMS data. We note that perturbations on a scale of 350 km are probably associated with gravity waves in Titan's upper atmosphere [Müller-Wodarg et al., 2006], whereas perturbations on a scale of 2000 km are likely to be induced by tidal waves in response to Saturn's gravity [e.g., Tokano and Neubauer, 2002; Strobel, 2006]. Therefore the INMS observations imply that the

density and temperature perturbations at Titan's exobase are not very likely to be caused by these effects.

[28] We show further with the solid line in Figure 6 the extreme case for which thermospheric perturbations propagate into the exosphere without damping. Mathematically, this corresponds to infinite size of exobase perturbations. However, this does not necessarily mean that the density and temperature fields on Titan's exobase tend to uniformity. Instead, it only represents the case in which a same level of variability (as the other models in the same figure) occurs on a very large spatial scale. Practically, the profile of H₂ density variability for such an extreme case can be obtained by (1) extracting random realizations of exobase conditions from the physical variations of H₂ density and N₂ temperature derived in section 2.2, (2) calculating the one-dimensional Chamberlain model with each pair of exobase H₂ density and exobase temperature from the random realization, and (3) determining the variance of different Chamberlain profiles at any given altitude. Reducing the two-dimensional problem to one-dimensional artificially ignores the effect of mixing as perturbations from different parts of the exobase propagate into the same exospheric region. Figure 6 shows that the model without damping is in reasonable agreement with the data. With the scale of exobase perturbations on Titan being constrained by the size of the satellite, this fact implies that the INMS observations of Titan's exospheric H₂ distribution cannot be interpreted by the traditional Chamberlain model assuming spatial perturbations. We investigate the validity of such a model in the following section, where we also provide a preferred interpretation of the INMS data.

4. Validity of the Approach

[29] In section 3, we use a three-dimensional collisionless model to estimate the H₂ density variability in Titan's exosphere. A comparison with the INMS data suggests that the exobase perturbations propagate well into the exosphere without damping. In addition to the Maxwellian VDF for H₂ at the exobase, two further assumptions are inherent in the model described in the previous section: (1) The H₂ molecules are collisionless above the exobase; (2) The observed variability is a spatial phenomenon. In this section, we examine the validity of these assumptions based on timescale considerations.

4.1. Collisional Effect

[30] The mean exobase temperature of ~ 141 K (see section 2.2) corresponds to a thermal velocity of ~ 1 km s⁻¹ for H₂ molecules. Adopting an H₂ scale height of ~ 1000 km in Titan's exosphere based on the INMS data [Cui *et al.*, 2008], this gives a dynamical timescale of $\sim 10^3$ s. In cases when the timescale for particle interaction involving H₂ is shorter than $\sim 10^3$ s, the effect of collision cannot be ignored in modeling Titan's exosphere. Some of the collisional effects have been estimated by Cui *et al.* [2008], including photoionization, photodissociation, electron impact ionization, as well as charge transfer with protons and/or O⁺ ions. These processes, serving as external loss mechanisms of H₂, are typically characterized by timescales in the range of 10^8 – 10^9 s, far exceeding the dynamical scale of $\sim 10^3$ s for H₂ molecules. Collisions with other major exospheric neutral species (N₂ and CH₄) and the chemical production/loss of H₂ are not

expected to be important either, due to the very low densities of the relevant species above Titan's exobase. As an example, the chemical loss time constant of H₂ at ~ 1400 km has been estimated to be $\sim 10^7$ s [Lavvas *et al.*, 2008]. Therefore we conclude that various collisional effects are not very likely to be responsible for the apparent disagreement between the model variability and observed variability in Titan's exospheric H₂ distribution (with the contribution from counting statistics removed), as shown in section 3.

[31] It is worth emphasizing that the collisional effect, even if non-negligible, does not necessarily counteract the damping of exobase perturbations as propagating into the exosphere. Due to the random nature of the distributions of H₂ density and neutral temperature at Titan's exobase (see section 2.1), the net effect of exospheric collisions could be either decreasing or enhancing the exospheric density variability, as compared to the ideal collisionless case.

4.2. The Effect of Temporal Perturbations

[32] In section 3, we describe the propagation of exobase perturbations into Titan's exosphere based on the assumption of spatial variability. In that case, the atmospheric structure is assumed to be roughly stationary during the time when the INMS data were acquired. In contrast, the density variability may also be interpreted in the temporal domain. In this case, the physical conditions over the exobase are assumed to be uniform at any given time. However, these conditions are not stationary and the observed variability in the exosphere is associated with the evolution of exobase density and temperature with time.

[33] The propagation of exobase perturbations into the exosphere is not instantaneous, but with a time delay determined by the dynamical timescale of particles following their Kepler trajectories above the exobase. The damping of exobase perturbations when propagating into the exosphere is induced by the difference in the particle travel time. Such a time delay effect was first proposed by Paul and Fahr [1979], in the context of atomic H distribution in the terrestrial exosphere. For Titan, the dynamical timescale of exospheric H₂ molecules is $\sim 10^3$ s (see section 4.1). Similar to the case assuming spatial perturbation, the determining factor in the framework of temporal variability is the timescale over which the exobase conditions vary. Exobase perturbations on timescales shorter than $\sim 10^3$ s are effectively damped in Titan's exosphere, while exobase perturbations on longer timescales are more easily preserved when propagating into the exosphere.

[34] We will not attempt a detailed numerical evaluation of the time delay effect in this paper, mainly due to two reasons. First, Figure 6 suggests that the INMS observations of the exospheric H₂ variability can be reasonably reproduced with the limiting case without damping. The calculation of such a limiting case does not rely on the assumption that the observed variability is spatial, thus the model assuming temporal variability gives essentially the same limiting case as well. With the typical dynamical timescale of $\sim 10^3$ s (see section 4.1), we can infer immediately that the INMS observations of H₂ variability in Titan's exosphere can be interpreted as a result of upward propagation of exobase perturbations on timescales longer than $\sim 10^3$ s. Second, for the altitude range considered here, the change in the profiles of exospheric density variability is not sensitive to the

detailed choice of the time constant for exobase perturbations, as long as this time constant is comparable with or longer than 10^3 s. This means that an accurate numerical calculation of the time delay effect does not help to constrain the exact timescale during which the physical conditions over Titan's exobase vary. However, the time interval between two consecutive flybys, with similar solar and geophysical conditions but significantly different density variations (see section 2.1), is typically ~ 1 Titan day, i.e., $\sim 1.4 \times 10^6$ s, which could be regarded as an upper limit to the timescale of thermospheric density and temperature perturbations on Titan. Based on the above reasonings, we suggest that the observed variability in Titan's H₂ exosphere reflects the time-varying structures in Titan's upper atmosphere and lower exosphere, with a possible timescale in the range of $\sim 10^3$ – 10^6 s. It is interesting to note that the above value is consistent with the thermal response time of ~ 10 Earth days predicted by the simulation of *Bell et al.* [2011] for Titan's upper atmosphere.

5. The Implications of Titan's Variable H₂ Exosphere

[35] In the framework of a collisionless model, we have considered two ideal cases for the propagation of exobase perturbations into Titan's exosphere, assuming that the observed variability is either spatial or temporal. In this sense, the degree that the exobase perturbations are damped in the exosphere is a diagnostic of either the spatial scale or temporal scale of atmospheric perturbations near Titan's exobase. In section 3, we show that the kinetic model of the spatial variability of H₂ in Titan's exosphere predicts considerably more damping than implied by the INMS data. This effectively rules out the possibility that the associated perturbations in Titan's upper atmosphere are induced by mechanisms such as gravity waves or tidal waves. Including rare collisions above Titan's exobase does not solve the problem (see section 4.1). In section 4.2, we further show that the INMS observations may be interpreted with the assumption of temporal variability. Along the above line of reasoning, we postulate the following scenario in interpreting the INMS observations: the physical conditions near or above Titan's exobase remain approximately uniform at any given time, but these conditions vary with time, characterized by a time constant in the range of $\sim 10^3$ – 10^6 s.

[36] We emphasize that the above conclusion does not necessarily contradict our previous works [*Müller-Wodarg et al.*, 2008; *Cui et al.*, 2009], which implicitly assume that the observed density/temperature variations in Titan's upper atmosphere reflect horizontally varying trends, as expected by TGCM model calculations. This is because (1) these two previous works are largely concentrated on thermospheric regions below the altitude levels considered here, and (2) *Müller-Wodarg et al.* [2008] have shown that the observed variations of INMS density and temperature tend to diminish toward Titan's exobase. The latter fact, along with the theoretical prediction that large ballistic flows in the exosphere tend to drive the density structure near or above the exobase toward uniformity [e.g., *Fahr*, 1970], support our postulation of a uniform exosphere on Titan.

[37] It is more likely that the actual variations in Titan's upper atmosphere and exosphere are a combination of both spatial and temporal effects, with the former possibly driven

by mechanisms such as atmospheric dynamics, and the latter possibly driven by mechanisms such as globally varying solar or magnetospheric inputs. Since at sufficiently high altitudes, spatial variability tends to be smoothed out by horizontal flows, we expect that temporal variability becomes dominant, as reflected in the INMS data of H₂ in Titan's exosphere. This is essentially associated with the fact that the spatial size of exobase perturbations is limited by the size of Titan, whereas no obvious restriction exists for the duration of temporal perturbations.

[38] Within the framework of any collisionless model, the temporal variability in Titan's exosphere is controlled by the time-varying density and temperature structures over the exobase, reflecting a variable upper atmosphere of the satellite. To explore whether this is driven by the varying amount of solar EUV/UV radiation or the varying level of magnetospheric particle precipitation into Titan's atmosphere, here we estimate a few relevant parameters, detailed as follows.

[39] 1. Exobase height: For each flyby in our sample, we estimate the exobase height, z_{exo} , with the definition of identical H₂ scale height and H₂ mean free path. The scale height, as a function of altitude, is obtained directly from the INMS H₂ density profile by taking the gradient of logarithmic H₂ density, and the calculation of the mean free path takes into account H₂-N₂ collision only, assuming hard sphere approximation. The values of z_{exo} are detailed in Table 1, with a mean of 1500 km and a variance of $\sim 5\%$. This validates our choice of the common exobase height in previous sections.

[40] 2. Escape flux: The H₂ escape flux referred to Titan's surface, F_s , is obtained by a diffusion model fitting for regions of Titan's upper atmosphere below the exobase (and down to the closest approach altitude of a given flyby), following the procedures of *Cui et al.* [2008]. More specifically, we solve for the H₂ diffusion equation with the escape flux treated as a free parameter to be constrained by comparing to the INMS density measurements of H₂. The values of F_s derived this way are listed in Table 1, characterized by a flyby-to-flyby variance of $\sim 10\%$ around a mean value of $\sim 1.1 \times 10^{10}$ cm⁻² s⁻¹. The variability in H₂ flux is small, as compared to the variability in either the exobase density/temperature or the total energy content within the H₂ exosphere (see below). In the case of pure Jeans escape, the exobase density should be anti-correlated with the exobase temperature to maintain a stable escape rate. Such an anti-correlation is indeed revealed by the data, as shown in Figure 7. The dashed line in the figure corresponds to a Jeans escape flux taken to be 1.1×10^{10} cm⁻² s⁻¹ referred to Titan's surface. The figure shows that the combination of n_{exo} and T_{exo} values for different flybys is in general consistent with the picture of thermal evaporation. However, it is worth mentioning that among 16 out of 24 flybys, for the measured value of the exobase density, the corresponding exobase temperature is considerably lower than the value required to sustain the Jeans flux, implying enhanced escape of H₂ on Titan. Such an enhancement has been interpreted by *Cui et al.* [2008] and *Strobel* [2009] as associated with an upward heat flow that modifies the Maxwellian VDF of H₂.

[41] 3. Total number of particles within the exosphere: For each flyby in our sample, we estimate the total number of H₂ molecules contained within the exosphere, N_{tot} , by integrating the INMS H₂ densities from the exobase up to 3500 km where the density value drops to a numerically insignificant

Table 1. Exobase Height (z_{exo}), Exobase Density (n_{exo}) and Temperature (T_{exo} , Derived From Isothermal Fitting), H₂ Escape Flux Referred to Titan's Surface (F_s), Total Number of Particles (N_{tot}) and Total Energy Content (E_{tot}) of Titan's H₂ Exosphere, Bulk Velocity of H₂ at the Exobase (u_{exo}), and Effective Size (L) and Mean Particle Energy (\hat{E}) of the H₂ Exosphere Estimated for Each Flyby in Our INMS Sample^a

| Flyby | z_{exo} (km) | n_{exo} (cm ⁻³) | T_{exo} (K) | F_s (cm ⁻² s ⁻¹) | N_{tot} | E_{tot} (erg) | u_{exo} (cm s ⁻¹) | L (km) | \hat{E} (eV) |
|----------|-----------------------|--------------------------------------|----------------------|---|----------------------|------------------------|--|----------|-----------------------|
| T5 | 1650 | 7.5×10^5 | 160 | 1.1×10^{10} | 2.6×10^{32} | -2.2×10^{19} | 5.4×10^3 | 1560 | -5.1×10^{-2} |
| T18 | 1450 | 1.5×10^6 | 128 | 1.1×10^{10} | 4.2×10^{32} | -1.0×10^{19} | 2.9×10^3 | 1360 | -1.5×10^{-2} |
| T21 | 1630 | 8.6×10^5 | 162 | 1.3×10^{10} | 2.5×10^{32} | -2.9×10^{18} | 5.8×10^3 | 1330 | -7.2×10^{-3} |
| T23 | 1480 | 9.6×10^5 | 148 | 1.1×10^{10} | 1.9×10^{32} | -1.6×10^{18} | 4.6×10^3 | 970 | -5.3×10^{-3} |
| T25 | 1690 | 6.5×10^5 | 178 | 1.1×10^{10} | 1.8×10^{32} | -6.2×10^{17} | 6.5×10^3 | 1170 | -2.2×10^{-3} |
| T26 | 1500 | 1.1×10^6 | 149 | 0.9×10^{10} | 2.9×10^{32} | -1.8×10^{18} | 3.4×10^3 | 1330 | -3.8×10^{-3} |
| T28 | 1470 | 1.0×10^6 | 144 | 1.0×10^{10} | 2.3×10^{32} | -3.1×10^{18} | 3.8×10^3 | 1070 | -8.7×10^{-3} |
| T29 | 1550 | 9.4×10^5 | 162 | 1.2×10^{10} | 2.3×10^{32} | -2.2×10^{18} | 5.0×10^3 | 1140 | -6.0×10^{-3} |
| T30 | 1520 | 8.3×10^5 | 157 | 1.2×10^{10} | 2.1×10^{32} | -2.4×10^{18} | 5.8×10^4 | 1180 | -7.2×10^{-3} |
| T32 | 1470 | 1.8×10^6 | 131 | 1.2×10^{10} | 4.7×10^{32} | -9.4×10^{18} | 2.8×10^3 | 1330 | -1.2×10^{-2} |
| T36 | 1550 | 7.5×10^5 | 188 | 1.3×10^{10} | 1.8×10^{32} | -1.2×10^{18} | 6.5×10^3 | 1150 | -4.2×10^{-3} |
| T39 | 1400 | 1.2×10^6 | 120 | 0.9×10^{10} | 2.3×10^{32} | -3.9×10^{18} | 3.1×10^3 | 920 | -1.1×10^{-2} |
| T40 | 1460 | 1.3×10^6 | 137 | 1.0×10^{10} | 3.1×10^{32} | -3.6×10^{18} | 3.1×10^3 | 1160 | -7.2×10^{-3} |
| T42 | 1530 | 1.0×10^6 | 161 | 1.3×10^{10} | 2.9×10^{32} | -3.1×10^{18} | 5.4×10^3 | 1390 | -6.6×10^{-3} |
| T43 | 1380 | 1.4×10^6 | 113 | 0.8×10^{10} | 2.6×10^{32} | -3.9×10^{18} | 2.6×10^3 | 950 | -9.1×10^{-3} |
| T48 | 1500 | 1.6×10^6 | 151 | 1.2×10^{10} | 3.6×10^{32} | -1.2×10^{19} | 3.0×10^3 | 1070 | -2.2×10^{-2} |
| T50 | 1460 | 2.0×10^6 | 135 | 1.1×10^{10} | 5.2×10^{32} | -9.4×10^{18} | 2.3×10^3 | 1260 | -1.1×10^{-2} |
| T56 | 1420 | 1.2×10^6 | 132 | 1.1×10^{10} | 3.1×10^{32} | -5.5×10^{18} | 3.8×10^3 | 1300 | -1.1×10^{-2} |
| T57 | 1520 | 1.0×10^6 | 150 | 1.4×10^{10} | 2.9×10^{32} | -4.4×10^{18} | 5.4×10^3 | 1390 | -9.3×10^{-3} |
| T58 | 1420 | 9.9×10^5 | 143 | 1.1×10^{10} | 2.6×10^{32} | -1.6×10^{18} | 5.0×10^3 | 1320 | -3.8×10^{-3} |
| T59 | 1470 | 1.5×10^6 | 140 | 1.0×10^{10} | 4.2×10^{32} | -5.7×10^{18} | 2.7×10^3 | 1360 | -8.5×10^{-3} |
| T61 | 1380 | 1.5×10^6 | 115 | 1.0×10^{10} | 3.1×10^{32} | -5.5×10^{18} | 2.9×10^3 | 1070 | -1.1×10^{-2} |
| T65 | 1520 | 1.5×10^6 | 154 | 1.0×10^{10} | 3.9×10^{32} | -5.2×10^{18} | 2.8×10^3 | 1310 | -8.0×10^{-3} |
| T71 | 1470 | 1.4×10^6 | 141 | 1.0×10^{10} | 3.4×10^{32} | -4.7×10^{18} | 2.7×10^3 | 1190 | -8.5×10^{-3} |
| Mean | 1500 | 1.2×10^6 | 146 | 1.1×10^{10} | 3.1×10^{32} | -5.2×10^{18} | 4.2×10^3 | 1220 | -1.0×10^{-2} |
| Variance | 5.3% | 29% | 13% | 13% | 30% | 88% | 34% | 13% | 92% |

^aNote that those flybys with data gaps near the exobase have been ignored (see section 2.1). The last two rows give the mean and the variation of each quantity over different flybys, where the variation is defined as the ratio of the standard deviation to the mean.

level. These values are also given in Table 1, indicating a variability of $\sim 30\%$ and a mean value of $\sim 3.1 \times 10^{32}$ particles. Accordingly, the total mass content is ~ 1000 tons on average.

[42] 4. Total energy content within the exosphere: A direct estimate of the total energy content of Titan's H₂ exosphere, E_{tot} , is more difficult as the exact form of the exospheric H₂ VDF is model dependent [e.g., Cui *et al.*, 2008]. Here for simplicity, we assume that the H₂ energy density scales exponentially with altitude above Titan's exobase, thus

$$E_{\text{tot}} \approx 4\pi r^2 H m n \left[c_p T_n - \frac{GM}{r} + \frac{1}{2} \left(\frac{F}{n} \right)^2 \right] \Big|_{\text{exobase}}, \quad (4)$$

where H and F are the H₂ scale height and flux, $c_p = 1.03 \times 10^8$ ergs K⁻¹ g⁻¹ is the H₂ specific heat, G is the gravitational constant, M is Titan's mass, and the other quantities have been defined above. All values are referred to Titan's exobase. Equation (4) combines the contributions from internal energy, gravitational energy and bulk kinetic energy of H₂ in Titan's exosphere. The values of E_{tot} estimated from equation (4) are detailed in Table 1, with their negative signs ensuring that the H₂ exosphere of Titan is gravitationally confined. The mean energy content is $\sim -5.2 \times 10^{18}$ ergs, with a variance as large as $\sim 90\%$.

[43] Table 1 shows a considerable variability in Titan's H₂ exosphere from flyby to flyby, especially in terms of the total energy content. The energy required to power Titan's H₂ exosphere ultimately comes from solar UV/EUV heating and/or magnetospheric energy deposition into the upper atmosphere. It is not very likely that the observed variability

in H₂ is driven by solar inputs only since the observations were made primarily under solar minimum conditions, with $\sim 10\%$ variance in solar activities based on either the F10.7 cm or 121.6 nm solar irradiance, reported by the space weather prediction center of the National Oceanic and Atmospheric Administration (NOAA). We state here, but do not show explicitly, that there is no obvious correlation between the

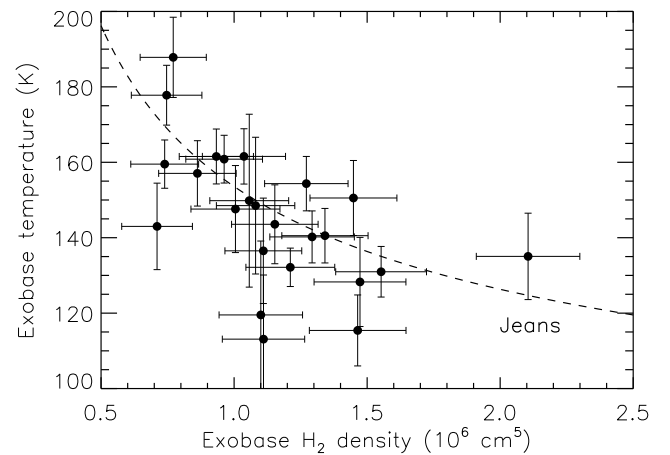


Figure 7. Exobase temperature as a function of exobase H₂ density. An anti-correlation between the two quantities is clearly present, which helps to maintain a relatively stable H₂ escape flux on Titan. The dashed line corresponds to the case of perfect Jeans escape with a fixed flux of 1.1×10^{10} cm⁻² s⁻¹ referred to Titan's surface.

Table 2. Mean Values of the Exobase Height (z_{exo}), Exobase Temperature (T_{exo}), H₂ Bulk Velocity at the Exobase (u_{exo}), Effective Size (L), and Mean Particle Energy (\hat{E}) Within the H₂ Exosphere, for Different Categories of Plasma Environment Near Titan

| Category | z_{exo} (km) | T_{exo} (K) | u_{exo} (cm s ⁻¹) | L (km) | \hat{E} (eV) |
|---------------|-----------------------|----------------------|--|----------|-----------------------|
| Lobe-like | 1400 | 122 | 8.0×10^3 | 1170 | -1.2×10^{-2} |
| Plasma sheet | 1500 | 151 | 1.2×10^4 | 1230 | -1.3×10^{-2} |
| Magnetosheath | 1500 | 146 | 1.0×10^4 | 1360 | -9.9×10^{-3} |

solar index (e.g., the F10.7cm solar irradiance) and any of the parameters calculated above. Based on the above considerations, and also motivated by existing results (especially those of *Westlake et al.* [2011]), we postulate that the observed H₂ variability is driven by the varying magnetospheric inputs into Titan's upper atmosphere.

[44] A highly variable plasma environment for Titan has recently been reported by *Rymer et al.* [2009], *Garnier et al.* [2010], and *Bertucci et al.* [2009], based on the in-situ data from the Cassini Plasma Spectrometer (CAPS), the Magnetosphere IMaging Instrument (MIMI), as well as the Cassini MAGnetometer (MAG). Distinct categories have been identified in terms of either the electron/proton energy spectrum or the magnetic field configuration. In a later work, *Westlake et al.* [2011] presented a preliminary analysis of the response of Titan's thermosphere to its varying plasma environment. Rough correlations have been found between different data sets. Especially, both the neutral temperature and the exobase height appear to be correlated with the level of electron precipitation from Titan's ambient plasma [*Westlake et al.*, 2011].

[45] To illustrate further the role of Titan's plasma environment on the H₂ exosphere, we investigate in particular those flybys with the plasma classification of PS (Plasma Sheet), L (Lobe-like) and MS (Magnetosheath) according to Table 2 of *Rymer et al.* [2009] and Table 1 of *Westlake et al.* [2011]. Typical CAPS electron spectra indicate a significantly lower suprathermal electron intensity for the L category as compared to the other two [*Rymer et al.*, 2009], implying less electron precipitation and energy deposition for the former case. A detailed comparison is provided in Table 2. For the 4 flybys classified as L (T18, T43, T56 and T61), the mean exobase height is $z_{\text{exo}} \approx 1400$ km and the mean exobase temperature is $T_{\text{exo}} \approx 122$ K. For the 8 flybys classified as PS (T5, T23, T29, T36, T39, T57, T58 and T59), $z_{\text{exo}} \approx 1500$ km and $T_{\text{exo}} \approx 151$ K, whereas for the remaining 2 flybys classified as MS (T32 and T42), $z_{\text{exo}} \approx 1500$ km and $T_{\text{exo}} \approx 146$ K. These variations for different plasma environments are essentially those found in the work of *Westlake et al.* [2011] based on a similar analysis method but a slightly different INMS sample [see also *Bell et al.*, 2011]. The trend in temperature indicates the additional heating from magnetospheric energy inputs in response to an enhanced level of electron precipitation into Titan's upper atmosphere. The variation of exobase height with the plasma environment implies a slight expansion of Titan's atmosphere associated with the extra heating.

[46] In terms of the escape flux, the total particle number as well as the total energy content of Titan's H₂ exosphere, it is more instructive to examine their values scaled by density than to compare directly their absolute values among different categories. Here we calculate the bulk velocity of H₂ at the

exobase, u_{exo} , the effective size, L , of the H₂ exosphere defined as $L = N_{\text{tot}} / (4\pi r_{\text{exo}}^2 n_{\text{exo}})$ with r_{exo} being the radius at the exobase and n_{exo} being the exobase H₂ density, as well as the mean particle energy, \hat{E} , within the exosphere defined as $\hat{E} = E_{\text{tot}} / N_{\text{tot}}$. These parameters are also detailed in Table 1. For the category of L, we find their mean values to be $u_{\text{exo}} \approx 8.0 \times 10^3$ cm s⁻¹, $L \approx 1170$ km and $\hat{E} \approx -1.2 \times 10^{-2}$ eV, for the category of PS, $u_{\text{exo}} \approx 1.2 \times 10^4$ cm s⁻¹, $L \approx 1230$ km and $\hat{E} \approx -1.3 \times 10^{-2}$ eV, whereas for the category of MS, $u_{\text{exo}} \approx 1.0 \times 10^4$ cm s⁻¹, $L \approx 1360$ km and $\hat{E} \approx -9.9 \times 10^{-3}$ eV. Therefore in general, with increasing amount of electron precipitation into Titan's atmosphere, the H₂ molecules in the exosphere gain more energy, expand further outward, and escape more rapidly from the satellite. The last feature does not necessarily contradict our previous results presented by *Cui et al.* [2008], where we proposed that the H₂ escape rate on Titan enhanced over the thermal Jeans value might be a result of upward heat flow in the upper atmosphere. In fact, the thermal structure (as well as the heat flow) in Titan's upper atmosphere may simply be modified by extra energy deposition from Titan's plasma environment, which finally leads to a varying level of H₂ escape.

[47] It is worth mentioning that *Strobel* [2010] suggested the presence of a downward H₂ flux into Titan's surface, in order to interpret simultaneously the INMS measurements of H₂ in Titan's upper atmosphere as well as the Voyager and Cassini infrared measurements of the same species in Titan's troposphere and lower stratosphere. Calculations show that the integrated downward H₂ flux is comparable to the integrated upward H₂ flux escaping out of the atmosphere [*Strobel*, 2010]. This implies that the integrated H₂ production rate should be doubled, as compared to the values predicted by existing photochemical models (in which the production of H₂ through CH₄ photolysis is balanced by the H₂ escape flux [e.g., *Lebonnois et al.*, 2003; *Lavvas et al.*, 2008; *Krasnopolsky*, 2009]). *Strobel* [2010] used this fact to imply an extra source of CH₄ destruction on Titan in addition to solar EUV/UV radiation, supposed to be magnetospheric particle precipitation. Therefore, we see that the two works on Titan's H₂ structure, though focused on different aspects, reach essentially a similar conclusion.

6. Concluding Remarks

[48] In this study, we investigate the structure of Titan's H₂ exosphere, based on the INMS neutral data acquired during 32 Cassini flybys with the satellite. No appreciable trend with solar or geophysical conditions has been identified in the distribution of H₂ above Titan's exobase. Despite this, there does exist a significant variance in H₂ density from flyby to flyby, which cannot be interpreted by counting statistics. The variability in exospheric H₂ density is calculated as a function of altitude, and is compared to predictions of the collisionless kinetic model, assuming that the variability is spatial. The degree that the H₂ variations are damped when propagating into Titan's exosphere depends on the spatial scale of the density and temperature perturbations over the exobase. However, detailed calculations show that all cases with realistic choices of this spatial scale cannot reproduce the data.

[49] An alternative point of view is to assume that Titan's exosphere remains roughly uniform globally, but may evolve

significantly with time, i.e., the observations of the H₂ variability should be interpreted as a temporal feature instead of a spatial one. In this case, the INMS data can be interpreted as a result of density and temperature perturbations over Titan's exobase varying with a timescale of $\sim 10^3$ – 10^6 s. This is in agreement with the time constant of ~ 10 Earth days predicted for the variations of thermal structure in Titan's upper atmosphere [Bell et al., 2011].

[50] Titan's variable H₂ exosphere essentially reflects the varying structure and energy deposition in the upper atmosphere of the satellite, which are ultimately driven by the variations in either the solar EUV/UV radiation or magnetospheric particle precipitation. However, the considerable variability observed for the exospheric H₂ density is not very likely to be associated with the varying solar inputs into Titan's atmosphere, since the data were primarily acquired under solar minimum conditions with a variance in solar irradiance only at $\sim 10\%$ level. We postulate that such a variability is probably associated with Titan's varying plasma environment. The requirement for magnetospheric inputs to interpret the H₂ structure on Titan has also been suggested recently by Strobel [2010], along a different line of reasoning.

[51] We also compare in detail the exospheric H₂ structure obtained for several different categories of Titan's plasma environment, based on the classification scheme of Rymer et al. [2009] and Westlake et al. [2011]. Both the exobase temperature and the exobase height tend to be lower for the lobe-like case, as compared to the plasma sheet case as well as the magnetosheath case. These features have recently been reported by Westlake et al. [2011]. Accordingly, with increasing level of energetic electron precipitation, Titan's H₂ exosphere appears to be more extended, more energetic, and H₂ molecules tend to escape more rapidly from the satellite. These features illustrate tentatively that the magnetospheric energy inputs from the ambient plasma may induce a noticeable effect on the structure of Titan's neutral upper atmosphere and lower exosphere.

[52] **Acknowledgments.** J.C. acknowledges support from the National Science Foundation of China through grant NSFC-11043016 to the National Astronomical Observatories affiliated to the Chinese Academy of Sciences. R.V.Y. acknowledges support from NASA through grant NAG5-12699 to the University of Arizona and sub-contract 699083KC from the Southwest Research Institute. I. M.-W. is funded by a University Research Fellowship of the British Royal Society. J.C. and M.G. acknowledge support from the Science and Technology Facilities Council (STFC) rolling grant to Imperial College London. We also thank Phillipe Garnier and the other anonymous referee, whose comments have significantly improved the paper.

[53] Masaki Fujimoto thanks the reviewers for their assistance in evaluating this paper.

References

- Ågren, K., et al. (2007), On magnetospheric electron impact ionization and dynamics in Titan's ram-side and polar ionosphere—A Cassini case study, *Ann. Geophys.*, *25*, 2359–2369, doi:10.5194/angeo-25-2359-2007.
- Bell, J. M., J. H. Westlake, and J. H. Waite Jr. (2011), Simulating the time-dependent response of Titan's upper atmosphere to periods of magnetospheric forcing, *Geophys. Res. Lett.*, *38*, L06202, doi:10.1029/2010GL046420.
- Bertucci, C., B. Sinclair, N. Achilleos, P. Hunt, M. K. Dougherty, and C. S. Arridge (2009), The variability of Titan's magnetic environment, *Planet. Space Sci.*, *57*, 1813–1820, doi:10.1016/j.pss.2009.02.009.
- Chamberlain, J. W. (1963), Planetary coronae and atmospheric evaporation, *Planet. Space Sci.*, *11*, 901–960, doi:10.1016/0032-0633(63)90122-3.
- Cravens, T. E., I. P. Robertson, S. A. Ledvina, D. Mitchell, S. M. Krimigis, and J. H. Waite Jr. (2008a), Energetic ion precipitation at Titan, *Geophys. Res. Lett.*, *35*, L03103, doi:10.1029/2007GL032451.
- Cravens, T. E., et al. (2008b), Model-data comparisons for Titan's night-side ionosphere, *Icarus*, *199*, 174–188, doi:10.1016/j.icarus.2008.09.005.
- Cui, J., R. V. Yelle, and K. Volk (2008), Distribution and escape of molecular hydrogen in Titan's thermosphere and exosphere, *J. Geophys. Res.*, *113*, E10004, doi:10.1029/2007JE003032.
- Cui, J., et al. (2009), Analysis of Titan's neutral upper atmosphere from Cassini Ion Neutral Mass Spectrometer measurements, *Icarus*, *200*, 581–615, doi:10.1016/j.icarus.2008.12.005.
- De La Haye, V., et al. (2007a), Cassini Ion and Neutral Mass Spectrometer data in Titan's upper atmosphere and exosphere: Observation of a suprathermal corona, *J. Geophys. Res.*, *112*, A07309, doi:10.1029/2006JA012222.
- De La Haye, V., J. H. Waite Jr., T. E. Cravens, A. F. Nagy, R. E. Johnson, S. Lebonnois, and I. P. Robertson (2007b), Titan's corona: The contribution of exothermic chemistry, *Icarus*, *191*, 236–250, doi:10.1016/j.icarus.2007.04.031.
- Fahr, H. J. (1970), Ballistical transport phenomena in a collision-free exosphere, *Planet. Space Sci.*, *18*, 823–834, doi:10.1016/0032-0633(70)90081-4.
- Garnier, P., I. Dandouras, D. Toublanc, E. C. Roelof, P. C. Brandt, D. G. Mitchell, S. M. Krimigis, N. Krupp, D. C. Hamilton, and J.-E. Wahlund (2010), Statistical analysis of the energetic ion and ENA data for the Titan environment, *Planet. Space Sci.*, *58*, 1811–1822, doi:10.1016/j.pss.2010.08.009.
- Hartle, R. E. (1973), Density and temperature distributions in non-uniform rotating planetary exospheres with applications to Earth, *Planet. Space Sci.*, *21*, 2123–2137, doi:10.1016/0032-0633(73)90187-6.
- Jacchia, L. G. (1971), Revised static models of the thermosphere and exosphere with empirical temperature profiles, *Smithson. Astrophys. Obs. Spec. Rep. No. 332*, Smithsonian Inst., Washington, D. C.
- Johnson, R. E., M. R. Combi, J. L. Fox, W.-H. Ip, F. Leblanc, M. A. McGrath, V. I. Shematovich, D. F. Strobel, and J. H. Waite Jr. (2008), Exospheres and atmospheric escape, *Space Sci. Rev.*, *139*, 355–397, doi:10.1007/s11214-008-9415-3.
- Kim, Y. H., and S. Son (2000), The effects of planetary rotation on the exospheric density distributions of the Earth and Mars, *J. Korean Astron. Soc.*, *33*, 127–135.
- Krasnopolsky, V. A. (2009), A photochemical model of Titan's atmosphere and ionosphere, *Icarus*, *201*, 226–256, doi:10.1016/j.icarus.2008.12.038.
- Lavvas, P. P., A. Coustenis, and I. M. Vardavas (2008), Coupling photochemistry with haze formation in Titan's atmosphere, Part II: Results and validation with Cassini/Huygens data, *Planet. Space Sci.*, *56*, 67–99, doi:10.1016/j.pss.2007.05.027.
- Lebonnois, S., E. L. O. Bakes, and C. P. McKay (2003), Atomic and molecular hydrogen budget in Titan's atmosphere, *Icarus*, *161*, 474–485, doi:10.1016/S0019-1035(02)00039-8.
- Magee, B. A., J. H. Waite Jr., K. E. Mandt, J. Westlake, J. Bell, and D. A. Gell (2009), INMS-derived composition of Titan's upper atmosphere: Analysis methods and model comparison, *Planet. Space Sci.*, *57*, 1895–1916, doi:10.1016/j.pss.2009.06.016.
- Meier, R. R., and P. Mange (1970), Geocoronal hydrogen: An analysis of the Lyman-alpha airglow observed from OGO-4, *Planet. Space Sci.*, *18*, 803–821, doi:10.1016/0032-0633(70)90080-2.
- Müller-Wodarg, I. C. F., and R. V. Yelle (2002), The effect of dynamics on the composition of Titan's upper atmosphere, *Geophys. Res. Lett.*, *29*(23), 2139, doi:10.1029/2002GL016100.
- Müller-Wodarg, I. C. F., R. V. Yelle, M. Mendillo, L. A. Young, and A. D. Aylward (2000), The thermosphere of Titan simulated by a global three-dimensional time-dependent model, *J. Geophys. Res.*, *105*, 20,833–20,856, doi:10.1029/2000JA000053.
- Müller-Wodarg, I. C. F., R. V. Yelle, N. Borggren, and J. H. Waite Jr. (2006), Waves and horizontal structures in Titan's thermosphere, *J. Geophys. Res.*, *111*, A12315, doi:10.1029/2006JA011961.
- Müller-Wodarg, I. C. F., R. V. Yelle, J. Cui, and J. H. Waite Jr. (2008), Horizontal structures and dynamics of Titan's thermosphere, *J. Geophys. Res.*, *113*, E10005, doi:10.1029/2007JE003033.
- Paul, G., and H. J. Fahr (1979), Propagation of the geomagnetic density and temperature effect into the exosphere, *Planet. Space Sci.*, *27*, 403–409, doi:10.1016/0032-0633(79)90116-8.
- Rymer, A. M., H. T. Smith, A. Wellbrock, A. J. Coates, and D. T. Young (2009), Discrete classification and electron energy spectra of Titan's varied magnetospheric environment, *Geophys. Res. Lett.*, *36*, L15109, doi:10.1029/2009GL039427.
- Sittler, E. C., R. E. Hartle, C. Bertucci, A. J. Coates, T. E. Cravens, I. S. Dandouras, and D. E. Shemansky (2010), Energy deposition processes in Titan's upper atmosphere and its induced magnetosphere, in *Titan*

- From Cassini-Huygens*, edited by R. H. Brown, J.-P. Lebreton, and J. H. Waite Jr., pp. 393–453, Springer, New York, doi:10.1007/978-1-4020-9215-2_16.
- Strobel, D. F. (2006), Gravitational tidal waves in Titan's upper atmosphere, *Icarus*, *182*, 251–258, doi:10.1016/j.icarus.2005.12.015.
- Strobel, D. F. (2009), Titan's hydrodynamically escaping atmosphere: Escape rates and the structure of the exobase region, *Icarus*, *202*, 632–641, doi:10.1016/j.icarus.2009.03.007.
- Strobel, D. F. (2010), Molecular hydrogen in Titan's atmosphere: Implications of the measured tropospheric and thermospheric mole fractions, *Icarus*, *208*, 878–886, doi:10.1016/j.icarus.2010.03.003.
- Tokano, T., and F. M. Neubauer (2002), Tidal winds on Titan caused by Saturn, *Icarus*, *158*, 499–515, doi:10.1006/icar.2002.6883.
- Vidal-Madjar, A., and J. L. Bertaux (1972), A calculated hydrogen distribution in the exosphere, *Planet. Space Sci.*, *20*, 1147–1162, doi:10.1016/0032-0633(72)90004-9.
- Vuitton, V., R. V. Yelle, and J. Cui (2008), Formation and distribution of benzene on Titan, *J. Geophys. Res.*, *113*, E05007, doi:10.1029/2007JE002997.
- Waite, J. H., Jr., et al. (2004), The Cassini Ion and Neutral Mass Spectrometer (INMS) investigation, *Space Sci. Rev.*, *114*, 113–231, doi:10.1007/s11214-004-1408-2.
- Westlake, J. H., J. M. Bell, J. H. Waite Jr., R. E. Johnson, J. G. Luhmann, K. E. Mandt, B. A. Magee, and A. M. Rymer (2011), Titan's thermospheric response to various plasma environments, *J. Geophys. Res.*, *116*, A03318, doi:10.1029/2010JA016251.
- Yelle, R. V., N. Borggren, V. De La Haye, W. T. Kasprzak, H. B. Niemann, I. C. F. Müller-Wodarg, and J. H. Waite Jr. (2006), The vertical structure of Titan's upper atmosphere from Cassini Ion Neutral Mass Spectrometer measurements, *Icarus*, *182*, 567–576, doi:10.1016/j.icarus.2005.10.029.

J. Cui, Department of Astronomy and Key Laboratory of Modern Astronomy and Astrophysics, Ministry of Education, Nanjing University, Nanjing 210093, China. (cuij@nao.cas.cn)

M. Galand and I. C. F. Müller-Wodarg, Space and Atmospheric Physics Group, Department of Physics, Imperial College London, Prince Consort Road, London SW7 2BW, UK.

P. P. Lavvas and R. V. Yelle, Lunar and Planetary Laboratory, University of Arizona, 1629 E. University Blvd., Tucson, AZ 85721, USA.